
CoLoRA: PARAMETER-EFFICIENT FINE-TUNING FOR CONVOLUTIONAL MODELS

A CASE STUDY ON OPTICAL COHERENCE TOMOGRAPHY CLASSIFICATION

Mariano Rivera Angello Hoyos

Centro de Investigación en Matemáticas, A.C. (CIMAT)
Guanajuato, Gto., 36240, Mexico
mrivera@cimat.mx

ABSTRACT

We introduce **CoLoRA** (Convolutional Low-Rank Adaptation), a parameter-efficient fine-tuning method for convolutional neural networks (CNNs). CoLoRA extends LoRA to convolutional layers by decomposing kernel updates into lightweight depthwise and pointwise components. This design reduces the number of trainable parameters by over 80% compared to conventional fine-tuning, preserves the original model size, and allows merging updates into the pretrained weights after each epoch, keeping inference complexity unchanged. On OCTMNISTv2, CoLoRA applied to VGG16 and ResNet50 achieves up to 1% accuracy and 0.013 AUC improvements over strong baselines (Vision Transformers, state-space, and Kolmogorov–Arnold models) while reducing per-epoch training time by nearly 20%. Results indicate that CoLoRA provides a stable and effective alternative to full fine-tuning for medical image classification.

Keywords Convolutional Neural Networks · Fine-tuning · Transfer Learning · LoRA · OCTMNISTv2

1 Introduction

Neural network models have grown dramatically in complexity and scale, particularly with foundational models such as GPT-4, LLaMA 3.2, and DeepSeek-V3, which contain tens to hundreds of billions of parameters [1, 2, 3]. This evolution underscores the need for efficient fine-tuning strategies that adapt pretrained models to downstream tasks without retraining the entire network. *Efficient Parameter Fine-Tuning* (EPFT) methods address this by freezing the backbone and training a small number of additional parameters, showing success in both vision and language [4, 5, 6]. Among these, LoRA is notable for simplicity and effectiveness. In medical imaging, adapter-based strategies also facilitate fine-tuning of transformer architectures such as SAM [7, 8]. Nevertheless, EPFT in medical imaging remains comparatively underexplored [9], where CNN-based transfer learning is still prevalent [10, 11].

Although CNNs are smaller than LLMs, effective fine-tuning remains crucial. Major challenges include overfitting, feature misalignment, and inefficient parameter adaptation—issues exacerbated when trainable parameters are numerous relative to available data [12]. Cross-domain transfer can suffer when source and target distributions differ substantially, and careful hyperparameter choices (learning rate, batch size, freezing policy) are needed to avoid catastrophic forgetting [13].

Rebuffi *et al.* proposed CNN adapters—residual modules that enable domain-specific adaptation while freezing the backbone [14, 15]. However, they permanently modify the architecture and increase inference cost. To address this, we propose **CoLoRA**, which extends LoRA to convolutional architectures by factorizing convolutional updates into pointwise (1×1) and depthwise components (Fig. 2b–c), enabling efficient fine-tuning without altering backbone parameters.

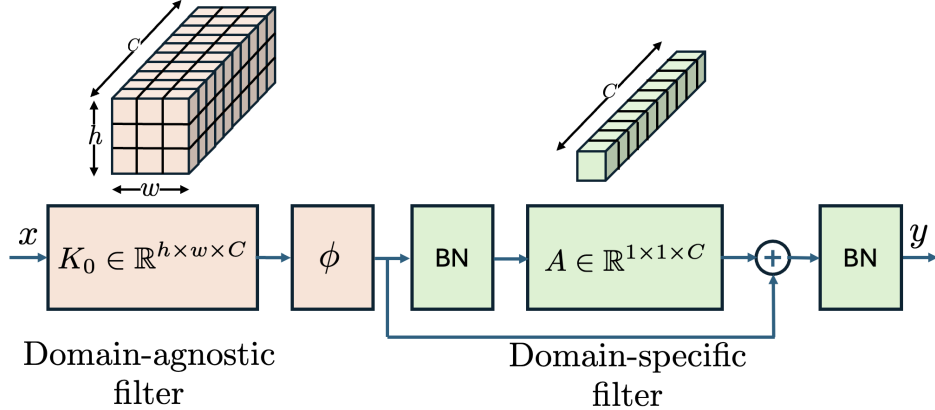


Figure 1: Schematic of Rebuffi’s CNN adapter. A 1×1 adapter after each convolutional block mixes preceding activations for domain-specific adaptation while freezing backbone filters.

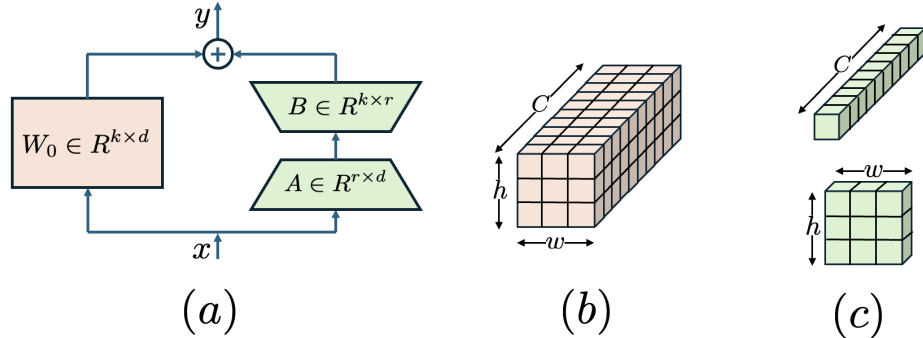


Figure 2: (a) LoRA on dense layers. (b) 2D convolutional kernel. (c) Depthwise–pointwise factorization of a 2D convolution.

We implement CoLoRA on VGG16 [16] and ResNet50 [17, 18], both ImageNet-pretrained. Inspired by Inception [19], we first capture cross-channel correlations to reduce tensor dimensionality, then model spatial correlations in the reduced representation. We evaluate on **OCTMNISTv2** [20, 21]—a clinically relevant, class-imbalanced benchmark (ChN, DME, Drusen, Normal) that remains challenging even for recent architectures [22, 23, 24]. CoLoRA-based CNNs match or surpass state of the art, with best accuracy 0.963 and AUC 0.95. The source code implementing CoLoRA is publicly available at: <https://github.com/ajhoyos/CoLoRA>

2 Related Methods

2.1 Convolutional Layers

A convolutional layer processes grid-structured data with learnable filters, extracting hierarchical spatial features [16, 17, 18, 25]. For $x \in \mathbb{R}^{H \times W \times C}$ and filter $K^t \in \mathbb{R}^{h \times w \times C}$ ($t = 1, \dots, T$), the output $y \in \mathbb{R}^{H \times W \times T}$ is

$$y(i, j, t) = (K^t \circledast x)(i, j) = \sum_{l, m, k} K^t(l, m, k) x(i + l, j + m, k). \quad (1)$$

2.2 CNN Adapters

CNN adapters [14, 15] introduce residual 1×1 modules trained while freezing the original filters. A simplified mechanism is:

$$y(i, j, t) = \sum_{k=1}^C A_{k, t} \phi((K^t \circledast x)(i, j)), \quad (2)$$

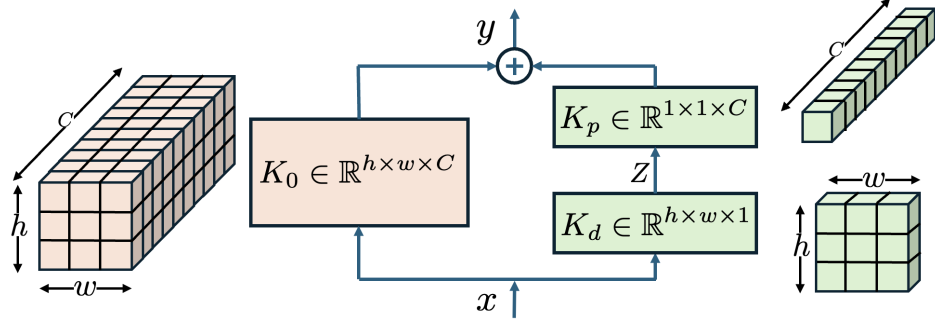


Figure 3: CoLoRA layer: a trainable depthwise–pointwise residual is added to a frozen convolution; updates are merged after training to preserve inference complexity.

where $A \in \mathbb{R}^{C \times T}$ is a 1×1 adapter and ϕ an activation. Since the feature subspace spanned by frozen filters is unchanged, features absent from the backbone cannot be recovered. CHAPTER [26] combines CNN adapters with transformer-style Houlsby adapters [27], improving flexibility but increasing inference cost.

2.3 LoRA: Low-Rank Adaptation

LoRA fine-tunes large models by adding low-rank updates while freezing backbone weights [28, 29, 30]. For a linear layer $y = W_0 x$, LoRA constrains $\Delta W = BA$ with $A \in \mathbb{R}^{r \times d}$ and $B \in \mathbb{R}^{k \times r}$, $r \ll \min(d, k)$:

$$y = (W_0 + \Delta W)x = W_0x + BAx. \quad (3)$$

Advantages include efficiency (fewer trained params), modularity (task-specific deltas), and scalability.

2.4 Separable Convolutional Layers

Depthwise separable convolutions, central to Xception and MobileNet [31, 32], factorize a standard convolution into depthwise and pointwise steps:

$$z(i, j, k) = (K_d \circledast x)(i, j, k) = \sum_{i', j'} K_d(i', j') x(i + i', j + j', k), \quad (4)$$

$$y(i, j) = (K_p \circledast z)(i, j) = \sum_k K_p(k) z(i, j, k), \quad (5)$$

which we summarize as $y = K_p \circledast (K_d \circledast x)$. This reduces parameters and FLOPs.

3 Proposed Method

CoLoRA extends LoRA to CNNs by constraining convolutional updates via a separable structure. Given a pretrained layer $y = K_0 \circledast x$, we introduce a residual update ΔK :

$$y = (K_0 + \Delta K) \circledast x = K_0 \circledast x + \Delta K \circledast x, \quad \Delta K = K_p \circledast K_d, \quad (6)$$

with pointwise K_p and depthwise K_d kernels (Fig. 3). We freeze K_0 and train only (K_p, K_d) (and optional bias Δb). Initialization uses Glorot-uniform for K_p , zeros for K_d (and Δb).

After training, we merge the updates:

$$K_0 \leftarrow K_0 + K_p \circledast K_d, \quad b_0 \leftarrow b_0 + \Delta b, \quad (7)$$

optionally at fixed intervals (e.g., after each epoch), yielding cumulative updates

$$K_0 \leftarrow K_0 + \sum_{e=1}^E K_p^{(e)} \circledast K_d^{(e)}, \quad b_0 \leftarrow b_0 + \sum_{e=1}^E \Delta b^{(e)}. \quad (8)$$

Thus, ΔK_0 lies in the span of $\{K_d^{(e)}\}$, capturing diverse spatial patterns accumulated over training.

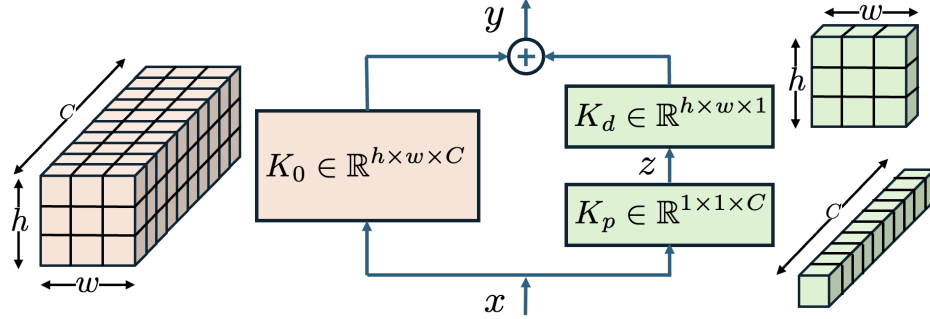


Figure 4: Inception-style CoLoRA: pointwise mixing precedes depthwise spatial filtering.

3.1 Generalization to Higher Dimensions

Because convolution is linear, we can swap the separable order:

$$\Delta K = K_d \circledast K_p, \quad (9)$$

first mixing channels (pointwise) then applying spatial filtering (depthwise), as in Inception [19, 31]; see Fig. 4. This generalizes naturally to 1D and 3D.

For 3D inputs $x \in \mathbb{R}^{H \times W \times D \times C}$:

$$z_1 = K_p \circledast x, \quad z_2 = K_d \circledast z_1, \quad z_3 = K_0 \circledast x, \quad y = z_3 + z_2. \quad (10)$$

Fig. 5 illustrates the 2D case.

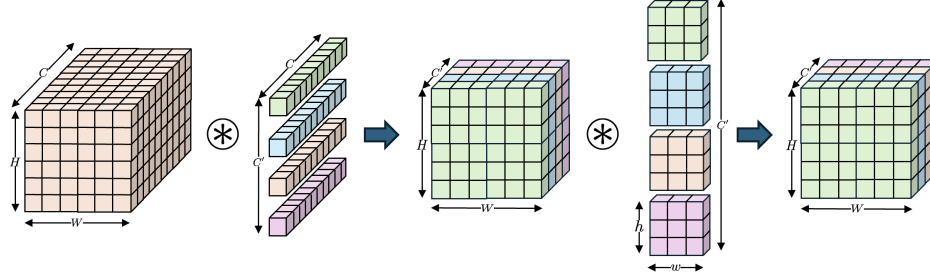


Figure 5: Operations of the CoLoRA layer (2D): 1×1 pointwise mixing per location followed by per-channel depthwise spatial convolution.

Convolution	Training	Inference
Original	$N_O = h w C T$	N_O
CNN Adapter	$N_A = C T + 2$	$N_O + N_A$
CoLoRA	$N_C = h w T + C T$	N_O

Table 1: Trainable parameter counts for a convolutional layer under different strategies. (h, w) : kernel size; C : input channels; T : filters. The CNN adapter includes BN (2 trainable parameters).

3.2 Implementation Details

We implemented CoLoRA on VGG16 [16] and ResNet50v2 [17], both pretrained on ImageNet. Each Conv2D in VGG16 was augmented with a CoLoRA bypass (Glorot for K_p , zeros for K_d). The head uses a 1×1 convolution ($512 \rightarrow 128$), then a dense layer (128 , ReLU) and a 4-way linear output.

The VGG16-CoLoRA model has ≈ 15.6 M parameters, of which ≈ 2.5 M are trained via backprop; updates are merged after each epoch. We use Adam (default settings) on an NVIDIA RTX 3090. An epoch took ~ 142 seconds.

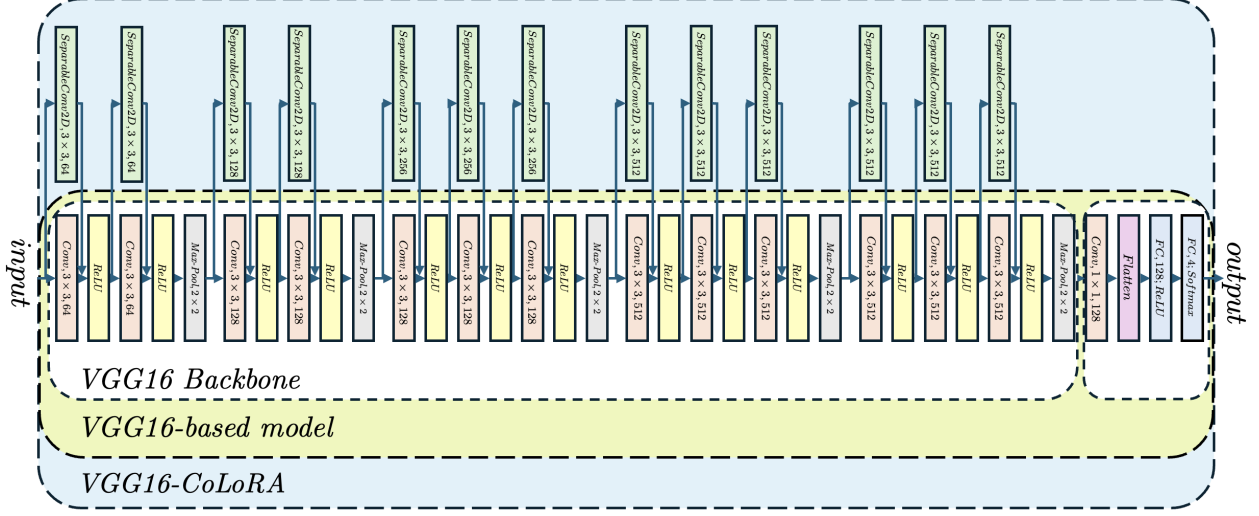


Figure 6: VGG16–CoLoRA architecture. Each convolution is augmented with a CoLoRA residual; the backbone is initialized from ImageNet.

4 Experiments

4.1 Dataset

We evaluate on OCTMNISTv2 [20, 21] (classes: ChN, DME, Drusen, Normal). OCT is widely used to diagnose and guide treatment in major retinal diseases [33]. The dataset is class-imbalanced (e.g., Drusen: 7,754 vs. Normal: 46,026). We use the data split into Train, Validation and Test as defined in the dataset. See Table 2.

Class	Index	Train	Val.	Test
ChN	1	33,484	2,708	250
DME	2	10,213	2,708	250
Drusen	3	7,754	2,708	250
Normal	4	46,026	2,708	250

Table 2: OCTMNISTv2 class counts by split.

To avoid confounds from heavy imbalance-handling, we construct a balanced training set by taking the first 7,754 samples (alphabetically sorted files names) from each class (31,016 total of 97,477).

4.2 Evaluation Metrics

Given the confusion matrix $C \in \mathbb{R}^{4 \times 4}$ with C_{ij} the number of true class i predicted as j :

$$\text{Recall}_i = \frac{C_{ii}}{\sum_j C_{ij}}, \quad (11)$$

$$\text{Precision}_i = \frac{C_{ii}}{\sum_j C_{ji}}, \quad (12)$$

$$\text{Accuracy} = \frac{\text{Tr}(C)}{\sum_{p,q} C_{pq}}. \quad (13)$$

For one-vs-rest analysis, the *specificity* for class i is

$$\text{Specificity}_i = \frac{\sum_{p \neq i} \sum_{q \neq i} C_{pq}}{\sum_{p \neq i} \sum_q C_{pq}}, \quad (14)$$

and ROC curves plot TPR_i vs. $FPR_i = 1 - \text{Specificity}_i$ as the decision threshold varies. The F1-score is

$$F1_i = \frac{2 \text{Precision}_i \text{Recall}_i}{\text{Precision}_i + \text{Recall}_i}. \quad (15)$$

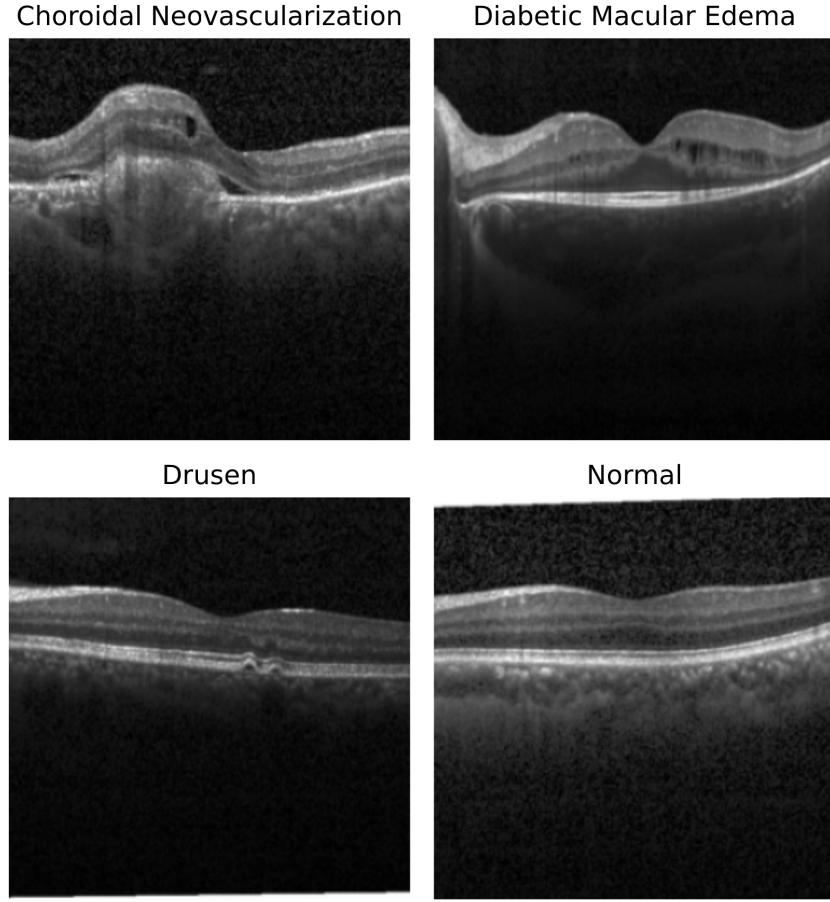


Figure 7: Representative OCTMNISTv2 images per class: ChN, DME, Drusen, and Normal.

4.3 VGG16–CoLoRA

We conducted **ten** independent runs for 20 epochs with random seed for the weights initialization. After each epoch, we merged CoLoRA updates, reset K_d and Δb to zero, and reinitialized K_p . We tracked loss/accuracy on train/val/test. Fig. 8 shows median (solid), IQR (dark band), and range (light band). Performance improves smoothly, with stable validation/test curves. We report the best test-epoch model per run. Confusion matrices and ROC curves are in Figs. 9 and 10. Classwise metrics (balanced set) appear in Table 3.

Class	AUC ROC	Recall	Precision	F1-score
ChN	0.992	0.972	0.927	0.949
DME	0.998	0.988	0.950	0.969
Drusen	0.983	0.932	0.971	0.951
Normal	0.999	0.948	0.995	0.971
Avg.	0.993	0.960	0.961	0.960

Table 3: VGG16–CoLoRA: class-wise metrics on the balanced training regime (test set).

We also perform entropy-based data distillation: for each class, discard the 10 highest-entropy items and retain the next 7,040. Fig. 11 shows sorted entropies; Figs. 12a–13b illustrate samples and predictions.

Table 5 compares CoLoRA to reference and recent SoTA models.

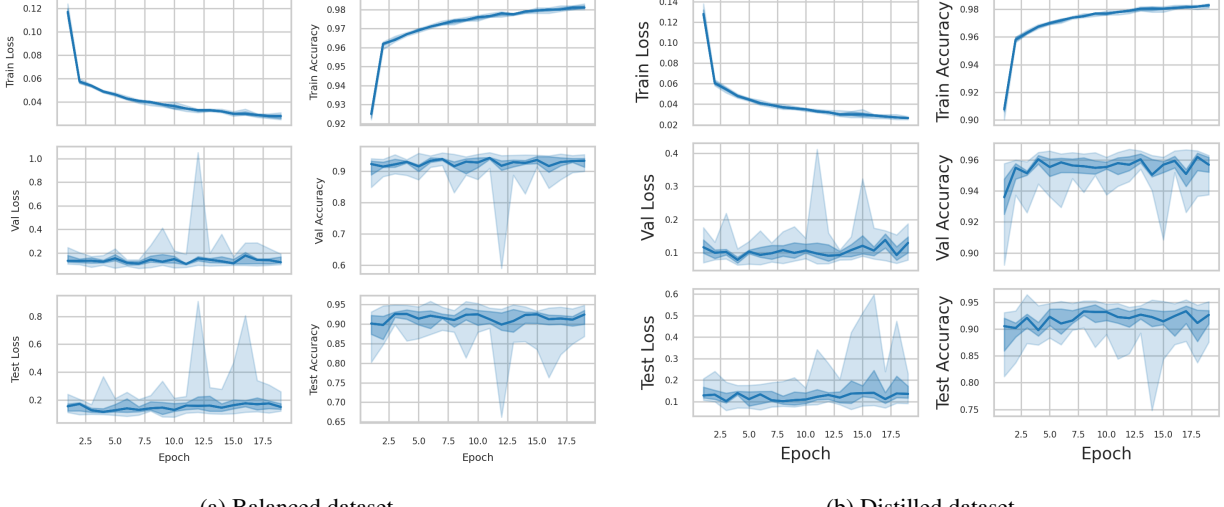


Figure 8: Learning curves (loss/accuracy) for VGG16–CoLoRA across **10** runs. Solid: median; dark band: IQR; light band: range.

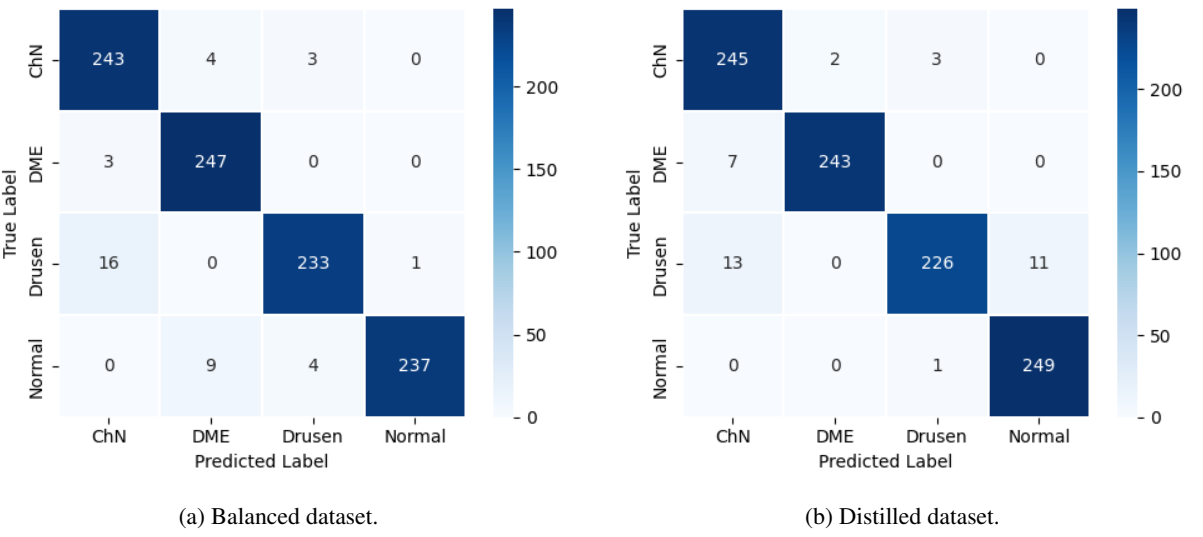


Figure 9: Confusion matrices on the OCTMNISTv2 test set for VGG16–CoLoRA.

Class	Transfer				CoLoRA			
	AUC	Rec.	Prec.	F1	AUC	Rec.	Prec.	F1
ChN	0.980	0.960	0.863	0.909	0.992	0.980	0.925	0.951
DME	0.983	0.932	0.955	0.943	0.999	0.972	0.988	0.980
Drusen	0.975	0.824	0.915	0.867	0.990	0.904	0.983	0.941
Normal	0.993	0.948	0.937	0.942	0.998	0.992	0.958	0.975
Avg.	0.983	0.916	0.918	0.915	0.995	0.962	0.963	0.962

Table 4: VGG16—Transfer vs. VGG16—CoLoRA on the distilled training set (test metrics).

4.4 ResNet50–CoLoRA

Under matched settings to VGG16, we first froze the ResNet50 backbone and trained only the head—this underperformed relative to [20]. Full fine-tuning improved accuracy to 0.903 but required training ~ 37 M parameters. With CoLoRA and a frozen backbone, selective CoLoRA layers achieved 0.951 accuracy, substantially improving efficiency

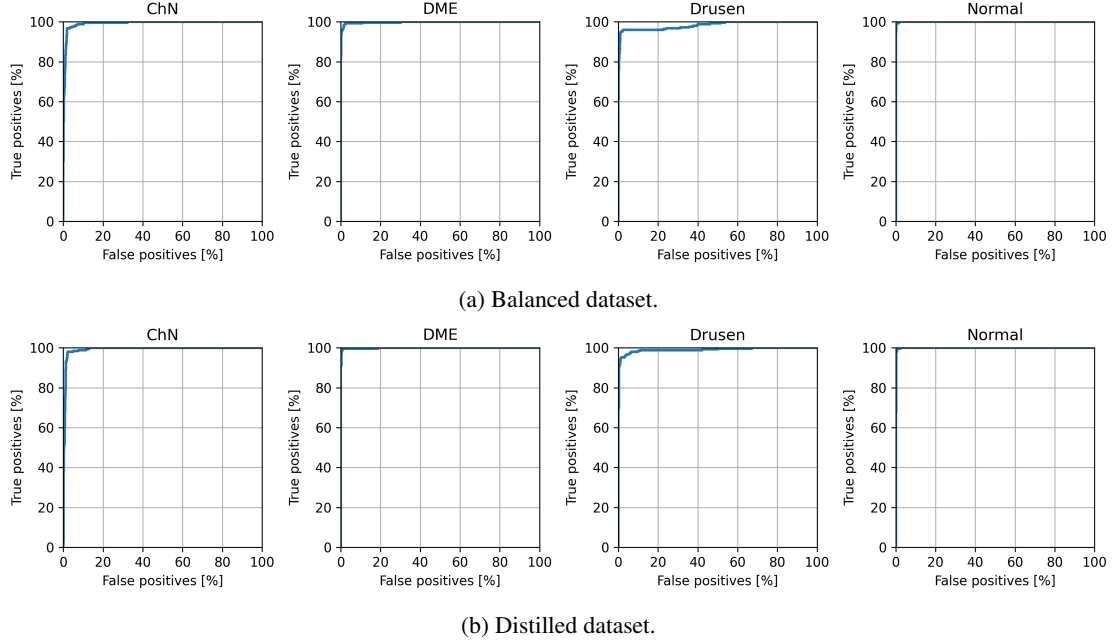


Figure 10: One-vs-rest ROC curves for VGG16–CoLoRA on OCTMNISTv2.

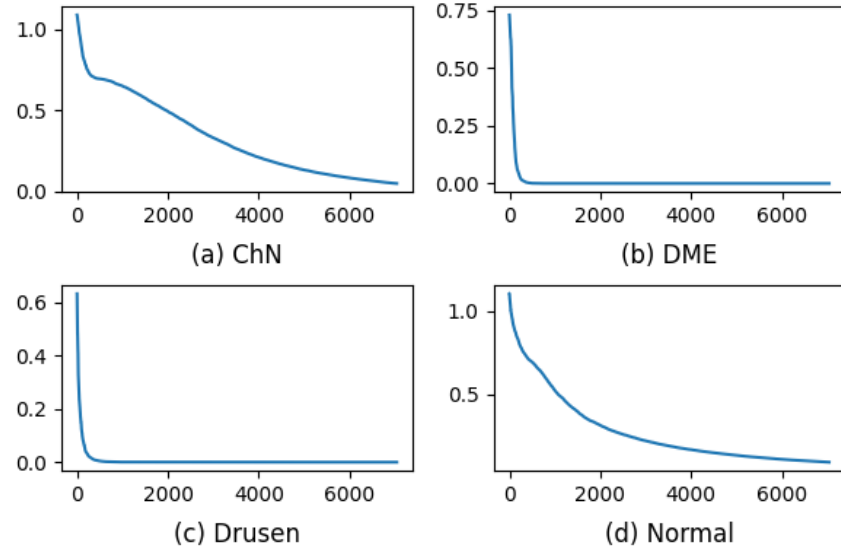


Figure 11: Sorted predictive entropy of distilled training samples (7,040 per class kept; top-10 highest-entropy per class discarded).

and performance. While strong, this did not surpass VGG16–CoLoRA’s best accuracy; future work will explore optimal CoLoRA placements across CNN families.

5 Conclusions

We presented **CoLoRA**, a parameter-efficient fine-tuning strategy that extends LoRA to CNNs by decomposing convolutional updates into depthwise and pointwise components. CoLoRA reduces trained parameters by >80% while preserving model size and inference complexity through epoch-wise merging. On OCTMNISTv2,

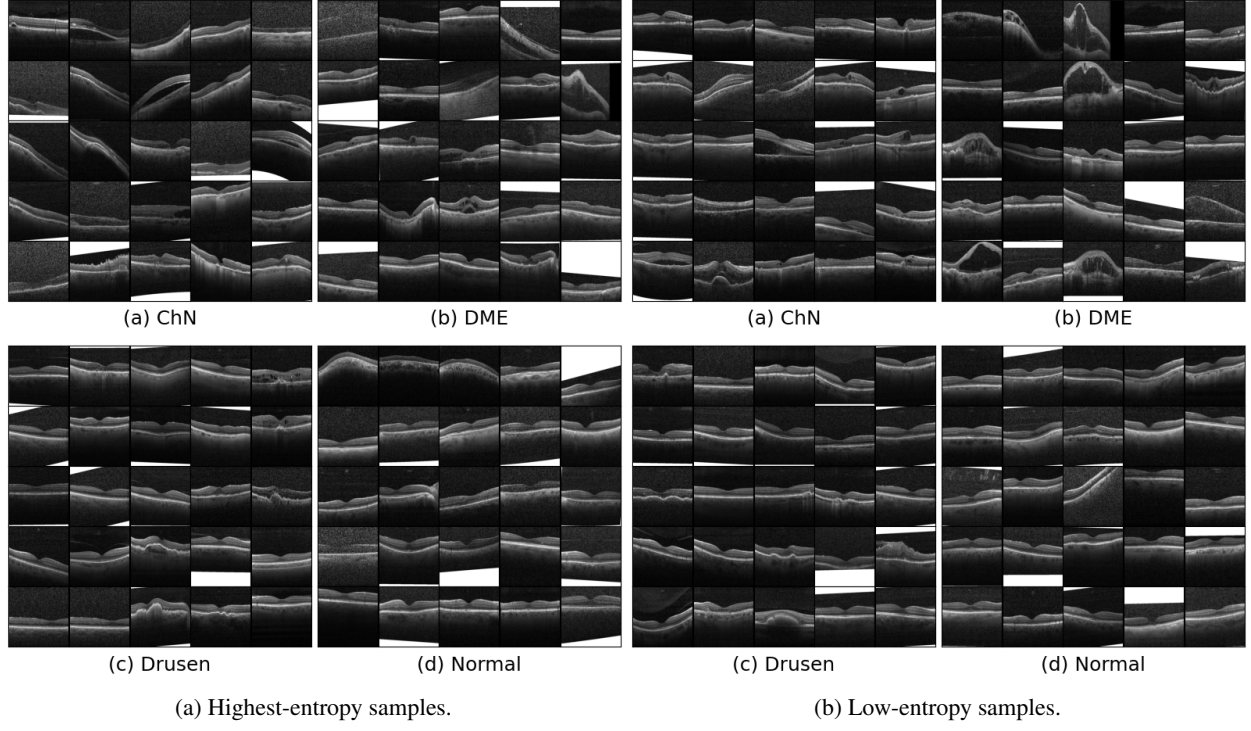


Figure 12: Examples grouped by predictive entropy used in distillation.

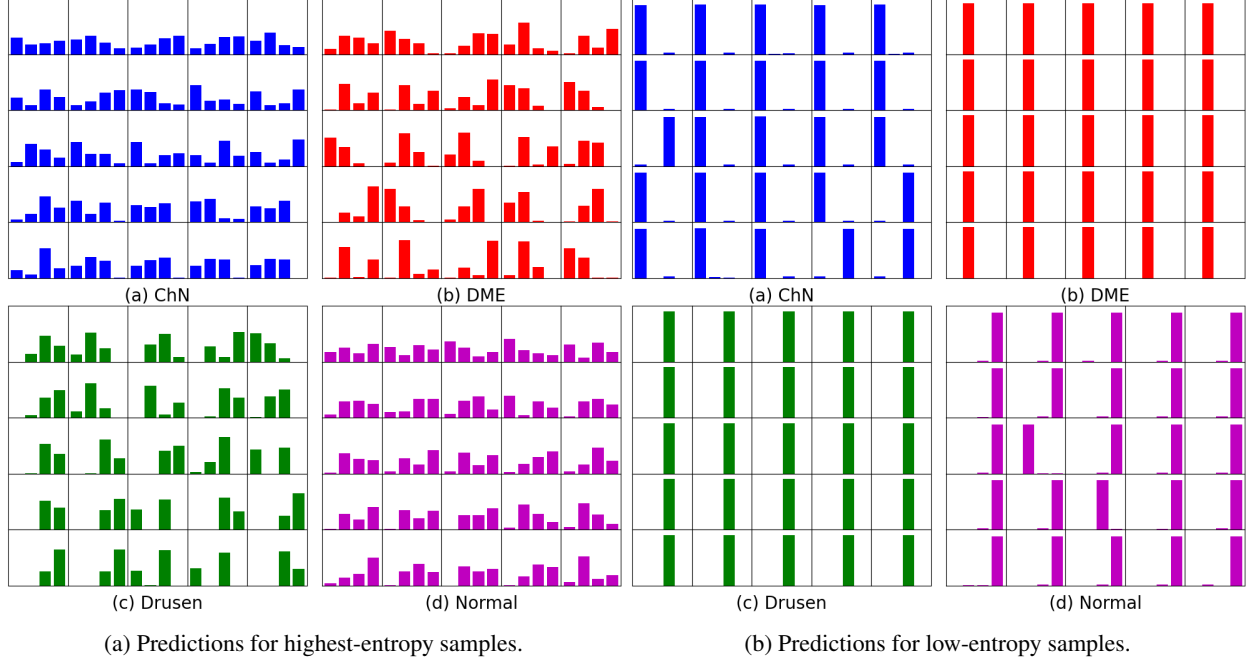


Figure 13: Predictions for entropy-grouped examples.

VGG16–ResNet50–CoLoRA achieved up to 1% accuracy and 0.013 AUC gains over strong baselines with $\sim 20\%$ faster training per epoch, demonstrating practical benefits in medical imaging.

Method	AUC	Acc.	Params.
ResNet-18 (28) [20]	0.951	0.758	
ResNet-50 (224) [20]	0.951	0.750	
Dedicated CNN (28) [34]		0.760	
ResNet-50 (224) [34]		0.776	
MedViTv1-T [22]	0.961	0.767	15.2M
MedViTv1-S [22]	0.960	0.782	
MedViTv1-L [22]	0.945	0.761	
MedKAN-S [24]	0.993	0.921	11.5M
MedKAN-B [24]	0.996	0.927	24.6M
MedKAN-L [24]	0.994	0.925	48.0M
MedMamba-T [35]	0.992	0.918	15.2M
MedMamba-S [35]	0.991	0.929	23.5M
MedMamba-B [35]	0.996	0.927	48.1M
MedMamba-X [35]	0.993	0.928	
MedViTv2-T [23]	0.993	0.927	
MedViTv2-S [23]	0.994	0.942	
MedViTv2-B [23]	0.996	0.944	32.3M
MedViTv2-L [23]	0.996	0.952	
ResNet50—Transfer Learning	0.983	0.903	37.7M
ResNet50— CoLoRA	0.992	0.951	14.2M [†]
VGG16—Transfer Learning	0.982	0.916	0.9M
VGG16— CoLoRA	0.995	0.963	2.6M [‡]

Table 5: Comparison on OCTMNISTv2. [†] 14.7M parameters trained by backprop out of 37.7M total. [‡] 2.5M trained by backprop out of 15.6M total.

Beyond quantitative gains, CoLoRA offers efficiency (few trained parameters), stability (separable residual updates), and deployability (unchanged inference footprint). It provides a flexible alternative to full fine-tuning for convolutional architectures.

6 Future Work

Future work will evaluate CoLoRA on larger, more heterogeneous datasets and additional modalities (fundus, dermoscopic, radiographic), extend to 1D/3D and spatiotemporal tasks (time series, volumetric OCT/CT/MRI), and explore integration with complementary parameter-efficient techniques (prompt tuning, adapter fusion, low-rank modulation). We will also study adaptive rank selection and dynamic merging schedules to optimize efficiency–accuracy trade-offs. These directions aim to consolidate CoLoRA as a general-purpose fine-tuning framework across domains, scales, and dimensionalities.

Acknowledgments. Work supported in part by SECTEI/CONAHCYT, Mexico (Grant CB-A1-43858).

References

- [1] C. Zhou, Q. Li, C. Li, J. Yu, Y. Liu, G. Wang, K. Zhang, C. Ji, Q. Yan, L. He, et al., A comprehensive survey on pretrained foundation models: A history from BERT to ChatGPT, *International Journal of Machine Learning and Cybernetics* (2024) 1–65.
- [2] D. Myers, R. Mohawesh, V. I. Chellaboina, A. L. Sathvik, P. Venkatesh, Y.-H. Ho, H. Henshaw, M. Alhawawreh, D. Berdik, Y. Jararweh, Foundation and large language models: fundamentals, challenges, opportunities, and social impacts, *Cluster Computing* 27 (2024) 1–26.
- [3] H. Naveed, A. U. Khan, S. Qiu, M. Saqib, S. Anwar, M. Usman, N. Akhtar, N. Barnes, A. Mian, A comprehensive overview of large language models, *arXiv preprint arXiv:2307.06435* (2023).
- [4] Z. Han, C. Gao, J. Liu, J. Zhang, S. Q. Zhang, Parameter-efficient fine-tuning for large models: A comprehensive survey, *Transactions on Machine Learning Research* (2024).

[5] N. Houlsby, A. Giurgiu, S. Jastrzebski, B. Morrone, Q. De Laroussilhe, A. Gesmundo, M. Attariyan, S. Gelly, Parameter-efficient transfer learning for NLP, in: K. Chaudhuri, R. Salakhutdinov (Eds.), Proceedings of the 36th International Conference on Machine Learning, volume 97 of *Proceedings of Machine Learning Research*, PMLR, 2019, pp. 2790–2799.

[6] J. Pfeiffer, A. Kamath, A. Rücklé, K. Cho, I. Gurevych, Adapterfusion: Non-destructive task composition for transfer learning, in: Proceedings of the 16th Conference of the European Chapter of the Association for Computational Linguistics: Main Volume, 2021, pp. 487–503.

[7] A. Kirillov, E. Mintun, N. Ravi, H. Mao, C. Rolland, L. Gustafson, T. Xiao, S. Whitehead, A. C. Berg, W.-Y. Lo, P. Dollar, R. Girshick, Segment anything, in: Proceedings of the IEEE/CVF International Conference on Computer Vision (ICCV), 2023, pp. 4015–4026.

[8] J. Wu, Z. Wang, M. Hong, W. Ji, H. Fu, Y. Xu, M. Xu, Y. Jin, Medical SAM adapter: Adapting segment anything model for medical image segmentation, *Medical Image Analysis* (2025) 103547. doi:<https://doi.org/10.1016/j.media.2025.103547>.

[9] R. Dutt, L. Ericsson, P. Sanchez, S. A. Tsaftaris, T. Hospedales, Parameter-efficient fine-tuning for medical image analysis: The missed opportunity, in: *Medical Imaging with Deep Learning*, 2024, pp. 406–425.

[10] H. E. Kim, A. Cosa-Linan, N. Santhanam, M. Jannesari, M. E. Maros, T. Ganslandt, Transfer learning for medical image classification: A literature review, *BMC medical imaging* 22 (2022) 69.

[11] A. W. Salehi, S. Khan, G. Gupta, B. I. Alabdullah, A. Almjally, H. Alsolai, T. Siddiqui, A. Mellit, A study of CNN and transfer learning in medical imaging: Advantages, challenges, future scope, *Sustainability* 15 (2023) 5930.

[12] S. Kornblith, J. Shlens, Q. V. Le, Do better imagenet models transfer better?, in: Proceedings of the IEEE/CVF conference on computer vision and pattern recognition, 2019, pp. 2661–2671.

[13] A. Kolesnikov, L. Beyer, X. Zhai, J. Puigcerver, J. Yung, S. Gelly, N. Houlsby, Large scale learning of general visual representations for transfer, *arXiv preprint arXiv:1912.11370* 2 (2019) 2019–4.

[14] S.-A. Rebuffi, H. Bilen, A. Vedaldi, Learning multiple visual domains with residual adapters, *Advances in neural information processing systems* 30 (2017).

[15] S.-A. Rebuffi, H. Bilen, A. Vedaldi, Efficient parametrization of multi-domain deep neural networks, in: Proceedings of the IEEE conference on computer vision and pattern recognition, 2018, pp. 8119–8127.

[16] K. Simonyan, Very deep convolutional networks for large-scale image recognition, *arXiv preprint arXiv:1409.1556* (2014).

[17] K. He, X. Zhang, S. Ren, J. Sun, Deep residual learning for image recognition, in: Proceedings of the IEEE Conference on Computer Vision and Pattern Recognition (CVPR), 2016, pp. 770–778.

[18] K. He, X. Zhang, S. Ren, J. Sun, Identity mappings in deep residual networks, in: *Computer Vision–ECCV 2016: 14th European Conference, Amsterdam, The Netherlands, October 11–14, 2016, Proceedings, Part IV* 14, Springer, 2016, pp. 630–645.

[19] C. Szegedy, W. Liu, Y. Jia, P. Sermanet, S. Reed, D. Anguelov, D. Erhan, V. Vanhoucke, A. Rabinovich, Going deeper with convolutions, in: Proceedings of the IEEE Conference on Computer Vision and Pattern Recognition (CVPR), 2015, pp. 1–9.

[20] J. Yang, R. Shi, B. Ni, MedMNIST classification decathlon: A lightweight AutoML benchmark for medical image analysis, in: *IEEE 18th International Symposium on Biomedical Imaging (ISBI)*, 2021, pp. 191–195.

[21] J. Yang, R. Shi, D. Wei, Z. Liu, L. Zhao, B. Ke, H. Pfister, B. Ni, MedMNIST v2-a large-scale lightweight benchmark for 2D and 3D biomedical image classification, *Scientific Data* 10 (2023) 41.

[22] O. N. Manzari, H. Ahmadabadi, H. Kashiani, S. B. Shokouhi, A. Ayatollahi, MedViT: A robust vision transformer for generalized medical image classification, *Computers in Biology and Medicine* 157 (2023) 106791.

[23] O. N. Manzari, H. Asgariandehkordi, T. Koleilat, Y. Xiao, H. Rivaz, Medical image classification with KAN-integrated transformers and dilated neighborhood attention, *arXiv preprint arXiv:2502.13693* (2025).

[24] Z. Yang, J. Zhang, X. Luo, Z. Lu, L. Shen, MedKAN: An advanced Kolmogorov-Arnold network for medical image classification, *arXiv preprint arXiv:2502.18416* (2025).

[25] R. Venkatesan, B. Li, *Convolutional neural networks in visual computing: A concise guide*, CRC Press, 2017.

[26] Z.-C. Chen, Y.-S. Sung, H.-y. Lee, Chapter: Exploiting convolutional neural network adapters for self-supervised speech models, in: *2023 IEEE International Conference on Acoustics, Speech, and Signal Processing Workshops (ICASSPW)*, IEEE, 2023, pp. 1–5.

- [27] N. Houlsby, A. Giurgiu, S. Jastrzebski, B. Morrone, Q. De Laroussilhe, A. Gesmundo, M. Attariyan, S. Gelly, Parameter-efficient transfer learning for NLP, in: International conference on machine learning, PMLR, 2019, pp. 2790–2799.
- [28] E. J. Hu, Y. Shen, P. Wallis, Z. Allen-Zhu, Y. Li, S. Wang, L. Wang, W. Chen, LoRA: Low-rank adaptation of large language models, in: International Conference on Learning Representations, 2022, pp. 1–13.
- [29] J. He, C. Zhou, X. Ma, T. Berg-Kirkpatrick, G. Neubig, Towards a unified view of parameter-efficient transfer learning, in: International Conference on Learning Representations, 2022, pp. 1–15.
- [30] J.-M. O. Steitz, S. Roth, Adapters strike back, in: Proceedings of the IEEE/CVF Conference on Computer Vision and Pattern Recognition, 2024, pp. 23449–23459.
- [31] F. Chollet, Xception: Deep learning with depthwise separable convolutions, in: Proceedings of the IEEE Conference on Computer Vision and Pattern Recognition (CVPR), 2017, pp. 1251–1258.
- [32] A. G. Howard, M. Zhu, B. Chen, D. Kalenichenko, W. Wang, T. Weyand, M. Andreetto, H. Adam, MobileNets: Efficient convolutional neural networks for mobile vision applications (2017), arXiv preprint arXiv:1704.04861 126 (2017).
- [33] N. Ferrara, Vascular endothelial growth factor and age-related macular degeneration: From basic science to therapy, *Nature Medicine* 16 (2010) 1107–1111.
- [34] M. Wilhelm, A. Rusiecki, Simple CNN as an alternative for large pretrained models for medical image classification-MedMNIST case study, *Procedia Computer Science* 239 (2024) 1298–1303.
- [35] Y. Yue, Z. Li, Medmamba: Vision mamba for medical image classification, arXiv preprint arXiv:2403.03849 (2024).